

# ON CROSS-TALK BETWEEN GYROSCOPES INTEGRATED ON A FOLDED MEMS IMU CUBE

Alexandra Efimovskaya<sup>1</sup>, Yu-Wei Lin<sup>1</sup>, Yushi Yang<sup>2</sup>, Eldwin Ng<sup>3</sup>, Yunnan Chen<sup>4</sup>, Ian Flader<sup>4</sup>,  
Chae H. Ahn<sup>3</sup>, Vu Hong<sup>5</sup>, Thomas W. Kenny<sup>4</sup>, and Andrei M. Shkel<sup>1</sup>

<sup>1</sup>MicroSystems Laboratory, University of California, Irvine, CA, USA

<sup>2</sup>Integrated Device Technology, Inc., San Jose, CA, USA <sup>3</sup>InvenSense, Inc., San Jose, CA, USA

<sup>4</sup>Stanford University, Palo Alto, CA, USA <sup>5</sup>Apple, Inc., Cupertino, CA, USA

## ABSTRACT

This paper reports a miniature Inertial Measurement Unit (IMU) implemented using a folded MEMS approach which allows for integration of high performance sensors, while providing a low cross-talk between the components. Foldable Si structures are manufactured on a wafer-level using MEMS techniques, co-fabricated or integrated with single-axis inertial sensors and then folded into a 3D configuration, forming the complete IMU. Electrical signals from the sensors on sidewalls of the IMU Cube are transferred through the dense network of metal traces on parylene, thus enabling the integration with signal processing electronics. For the first time, we characterized cross-talk between sensors on a folded 3D IMU. The experimental results provided an evidence that the folded IMU process is advantageous to a single-die approach, showing a lower Angle Random Walk (ARW) of the gyroscopes when operated simultaneously on different sidewalls of the IMU Cube.

## INTRODUCTION

During the last decade, there was an increasing demand for small, yet high performance, inertial measurement instruments. To meet this requirement a variety of MEMS-based IMUs emerged in recent years [1]- [8]. There are currently two status quo fabrication approaches for IMU implementation: (1) a manual assembly of 6 inertial sensors and (2) implementation of all 6 inertial sensors on a single chip. The first solution utilizes off-the-shelf single-axis sensors, manually assembled into a 3D configuration. The approach allows for improved performance, but often results in increased size and weight of the system. In contrast, a single-chip solution delivers an advantage of small volume at the cost of sub-optimal performance due to utilization of a single structural layer, potentially resulting in an increased cross-talk. Realization of high performance IMU in a compact form-factor remains to be a challenge.

An alternative approach is a Folded MEMS process [9]. It utilizes an array of single-axis sensors fabricated on a wafer-level and subsequently folded into a 3D IMU configuration using integrated flexible polymer hinges. This permits a significant reduction in size without a compromise in device performance. The folded IMU with polyimide flexible hinges and in-situ fabricated sensors was previously demonstrated in [10]. In this paper, we present, for the first time, a fabrication process for foldable structures with parylene hinges, metal traces on parylene, and Ni-reinforced electrical contact pads,

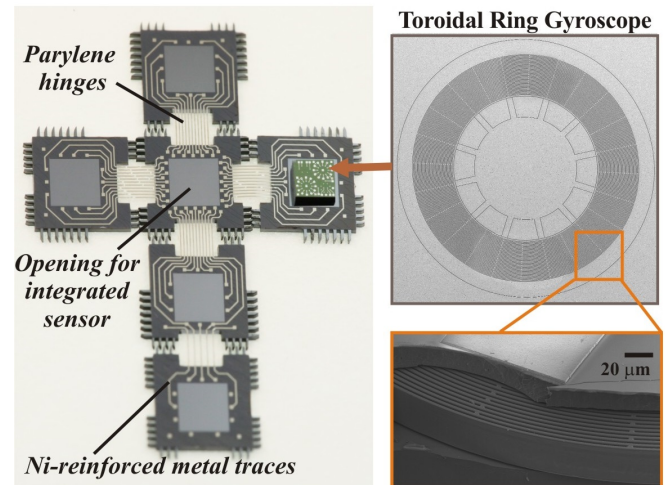


Figure 1: Foldable MEMS structures integrated with stand-alone single-axis Toroidal Ring Gyroscopes [12], implemented in Epi-Seal process.

all are the critical features of the folded IMU. In order to illustrate the advantage of the folded MEMS approach, a miniature IMU implemented using a foldable Si backbone was integrated with stand-alone silicon encapsulated sensors [11] and the cross-talk between sensors was characterized.

## FABRICATION

The foldable Si backbone can be fabricated using the process flow in Fig.2.1 for Ni-reinforced metal traces on parylene, or using the process flow in Fig.2.2 for Ni-reinforced contact pads and gold traces on parylene. In both cases, the fabrication starts with deposition of a Cr adhesion layer and a 16  $\mu\text{m}$  thick film of parylene-C, Fig.2.1(a) and Fig.2.2(a). The flexible hinges are photo-lithographically defined, and the parylene is etched using the RIE process with a Ti mask, Fig.2.1(b) and Fig.2.2(b).

Metal traces are created using E-Beam evaporation of the Cr layer (50 nm) and the Au layer (0.5  $\mu\text{m}$ ), Fig. 2.1(c). Next, the wafer is spin-coated with a thick layer of photoresist and the metal traces features are defined. A wafer-level electroplating method is then used to cover the areas of the wafer, free of the photoresist, with a 0.7  $\mu\text{m}$  thick layer of Ni, Fig.2.1 (c). This is followed by stripping the photoresist in acetone and wet-etching the Au and Cr layers using the electroplated Ni as a mask, Fig.2.1(d). Ni electroplating

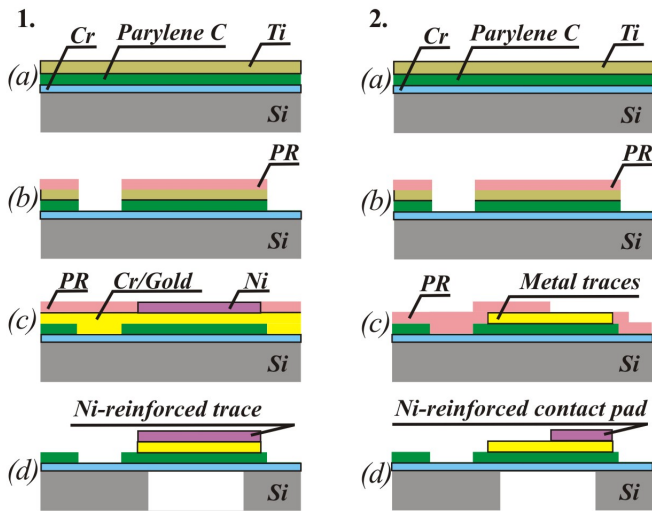


Figure 2: Process flow for foldable structures with 1: Ni-reinforced metal traces on parylene; 2: Ni-reinforced contact pads and gold traces on parylene.

allows for increased thickness and hardness of metal. This enables reinforcement of metal traces and contact pads thereby assuring the increased reliability of the wire-bond connections to the electrical contact pads on parylene. The backside thru-wafer Si etch completes the process, Fig.2.1(d).

Alternatively, Ni electroplating can be used for reinforcement of contact pads only. The Cr layer (50 nm) and the Au layer (0.5  $\mu\text{m}$ ) are first deposited using E-Beam evaporation and the metal traces features are defined, Fig. 2.2(c). Next, the wafer is spin-coated with a thick layer of photoresist, the electrical contact pads are defined and covered with a 0.7  $\mu\text{m}$  thick layer of Ni, using wafer-level electroplating method, Fig. 2.2(d). The backside thru-wafer Si etch completes the process, Fig.2.2(d).

The method of contact pads reinforcement, where only the pads are covered with Ni, is preferable for miniature IMU (<15  $\text{mm}^3$ ) since electroplating of the full length of traces results in partial delamination of thick traces from parylene during folding. However, for the 50  $\text{mm}^3$  IMU presented in this paper, the method of reinforcement using electroplating of the full length of traces was chosen. It has an advantage of the simplified process flow where one of the lithography steps is eliminated. For the IMU prototypes of this volume, the delamination of Ni-reinforced traces was not observed.

The stand-alone Toroidal Ring Gyroscopes (TRG) [12] were fabricated using a wafer-level Epitaxial Silicon Encapsulation (Epi-Seal) process [11]. In this process, movable silicon microstructures are encapsulated with a layer of epitaxially deposited silicon, allowing for an ultra-clean hermetic seal and resulting in high vacuum environment without the need for getter materials for absorption of sealing by-products. During the last years, the Epi-Seal process found many applications, including MEMS resonators and high Q-factor miniature angular rate sensors.

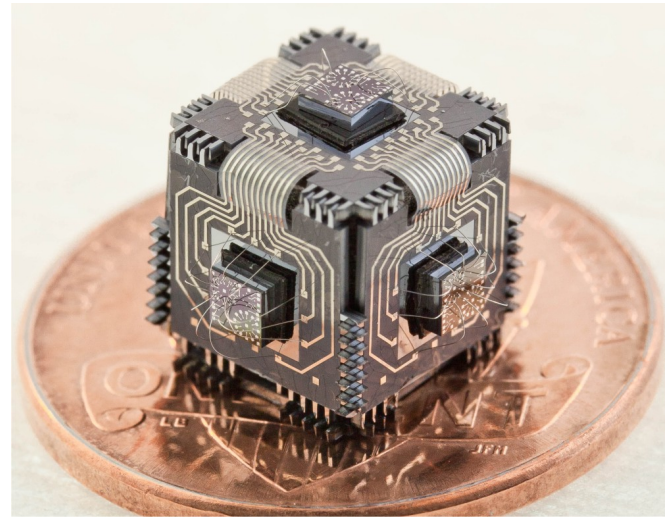


Figure 3: Folded 3D IMU on a coin of US cent (for size reference). A die with two TRGs is integrated on each sidewall.

## EXPERIMENTAL RESULTS

### Frequency Response Characterization

Fabricated IMU prototypes were folded into a 3D Cube configuration, Fig.3. A die with two TRGs and one accelerometer was integrated on each sidewall of the Folded IMU structure. IMU devices were die-attached to an adapter board, packaged into a 181-pin, gold plated Ceramic Pin Grid Array (CPGA) package, and assembled with front-end electronics. Electrical connections between sensors on the IMU sidewalls and the package are realized using metal traces on parylene and wire-bonds between the device and Ni-reinforced contact pads.

Characterization of the TRGs before and after IMU integration confirmed the feasibility of the electrical conduc-

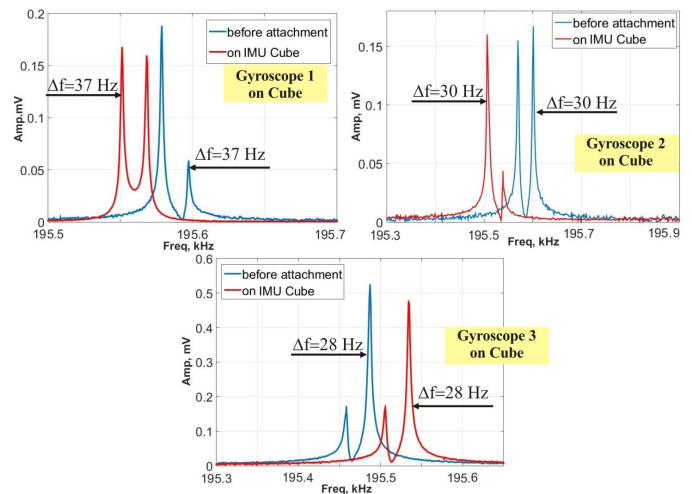


Figure 4: Frequency sweeps of TRGs before (blue line) and after (red line) integration on a Folded Cube.

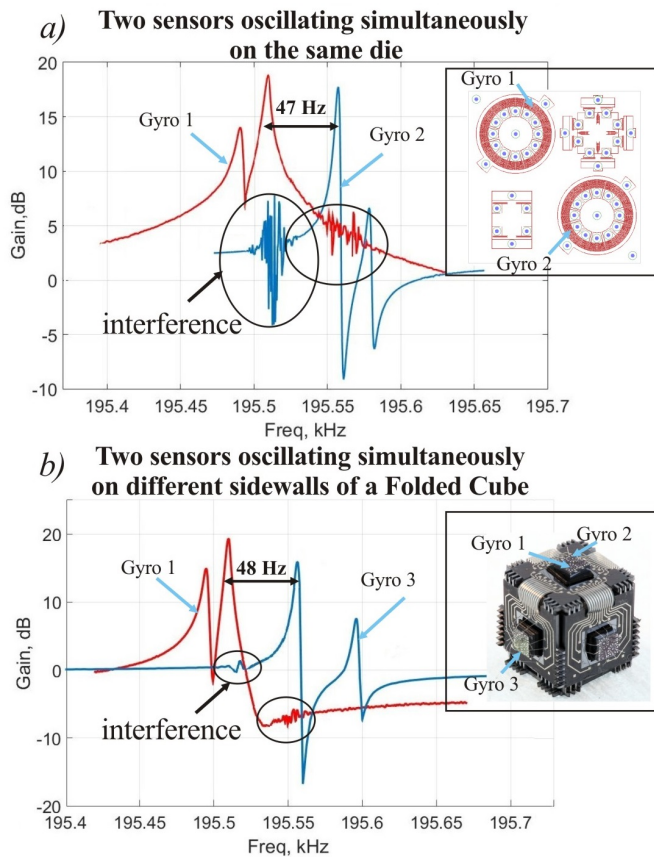


Figure 5: Higher level of interference of two sensors on the same die(a) vs on different sidewalls of the Cube(b).

tion method utilizing metal traces on parylene, Fig.4. The observed shift in resonance frequency is related mainly to the die-attachment stresses and temperature drift between the two subsequent tests.

### Cross-Talk Characterization

Cross-talk between the individual sensors in IMU contributes to the scale factor errors and results in the increased noise, effecting the IMU performance. In case of MEMS vibratory sensors, the mechanical cross-talk, as well as the electrical cross-talk, have to be considered.

The mechanical cross-talk originates from the vibration propagation through the substrate, in case of a single-die IMU, and through the Cube sidewalls, in case of the Folded Cube approach. The electrical cross-talk is a result of capacitive and/or resistive coupling. In order to suppress the electrical cross-talk on the Printed Circuit Board (PCB) level, the front-end electronics circuits of devices operating at close frequencies, were separated. In a single-die IMU, the electrical cross-talk arises from capacitive coupling of the very closely spaced wire bonds and capacitive/resistive coupling through the substrate. The main source of the electrical cross-talk in the Folded IMU is the capacitive coupling between the metal traces on parylene.

The study of cross-talk between the sensors was per-

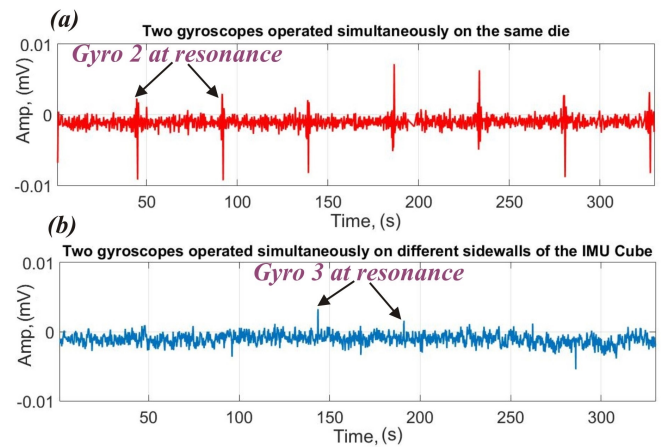


Figure 6: Zero-rate output of Gyro1: Higher level of interference of two sensors on the same die(a) vs on different sidewalls of the Cube(b).

formed using frequency domain characterization of two gyroscopes on the same die, Fig.5 (a), and two gyroscopes on different sidewalls of the IMU Cube, Fig.5 (b). The frequency response of the first gyroscope was obtained during the continuous oscillation of the second gyroscope at its own resonant frequency. In our experiments, all gyroscopes were excited with a 2.4 V constant DC voltage and a 100 mV AC voltage. Crosstalk normally occurs when the operating frequencies of the sensors in IMU are close to each other. Frequency split between the two gyroscopes on the same die was 47 Hz and was similar to the frequency split between the two gyroscopes on different sidewalls of the Cube (48 Hz).

Experimental frequency response characterization of the first gyroscope indicated the interaction between sensors, which was observed around the resonant frequency of the second gyroscope. Experimental testing revealed a significantly higher level of interference of two sensors on the same die as compared to two sensors on different sidewalls of the Folded Cube (11.5 dB versus 2 dB).

Cross-talk between sensors affected the zero-rate output of the gyroscope 1, Fig. 6. In this experiment, the gyroscope 1 was excited with a constant DC voltage and AC voltage generated by a Phase Locked Loop. The amplitude of the drive-mode motion was stabilized, using an Automatic Gain Control (AGC). Gyroscopes 2 (on the same die) and 3 (on different sidewall) were excited with a constant DC voltage and AC voltage with a frequency of the drive signal in the range from 195.45 kHz to 195.65 kHz. High level peaks (approximately 15 dB) were observed on the zero-rate output of gyroscope 1, when the driving frequency of the gyroscope 2 reached the resonance. A significantly lower level of cross-talk (< 4 dB) was observed on the zero rate response of the gyroscope 1, when gyroscope 3 was excited.

The Root Allan Variance Analysis (r-AVAR) was used for identification of random noise characteristics of the gyroscope 1. The interference between gyroscopes 1 and 2, on the same die, affected the noise of sensors and reflected on

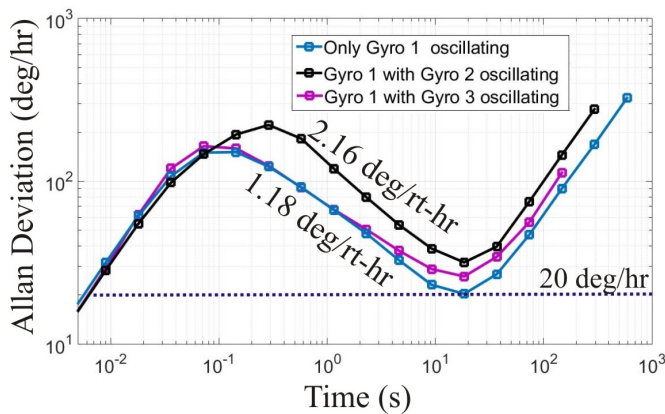


Figure 7: Interference between sensors results in higher ARW of Gyro1 with Gyro2 oscillating on a same die.

an Allan deviation plot, resulting in increased Angle Random Walk (ARW), from 1.18 to 2.16  $\text{deg}/\sqrt{\text{hr}}$ , and higher Rate Random Walk (RRW) of the gyroscope 1, Fig. 7. Noise analysis of the gyroscope 1 in presence of the gyroscope 3, oscillating on the other sidewall of a Cube, revealed nearly no change in ARW and lower RRW. This suggests that the Folded IMU approach allows for lower cross-talk between the sensors as compared to a single-die approach.

## CONCLUSIONS

We presented a miniature Inertial Measurement Unit (IMU) implemented using a folded MEMS technique. The approach is based on folding an array of single-axis inertial sensors into a 3D IMU configuration, using polymer flexible hinges. We presented a novel fabrication process for foldable structures with parylene hinges connecting the Si panels, metal traces on parylene, and Ni-reinforced electrical contact pads. Fabricated Folded IMU prototypes were integrated with stand-alone sensors fabricated in Silicon Encapsulated (Epi-Seal) process. The frequency response analysis of the gyroscopes before and after IMU integration confirmed the feasibility of the electrical conduction method.

In order to demonstrate advantages of the folded IMU approach, we analyzed the performance of gyroscopes operating on a same die and on the different sidewalls of a Folded Cube. The study of cross-talk between the simultaneously operating sensors was performed using frequency domain characterization, gyroscopes zero rate output, and noise characterization. Experimental frequency response and a zero rate output of the gyroscopes showed a higher level of interference between two sensors on the same die vs on different sidewalls of the Folded Cube. Experimental testing proved an advantage of a folded IMU as compared to a single-die approach, showing a lower angle random walk (ARW) of the two gyroscopes simultaneously oscillating on different sidewalls of a Folded IMU Cube, 1.18 vs 2.16  $\text{deg}/\sqrt{\text{hr}}$ .

## ACKNOWLEDGEMENTS

This material is based upon work supported by DARPA grant N66001-13-1-4021. Devices were designed, developed,

and tested at MicroSystems Laboratory, UC Irvine.

## REFERENCES

- [1] Honeywell, “HG1930 IMU”, [www.honeywell.com](http://www.honeywell.com), (2012).
- [2] Systron Donner, “SDI500 Tactical Grade IMU”, [www.systron.com](http://www.systron.com) (2014).
- [3] Northrop Grumman, “MEMS IMU”, [www.northropgrumman.litef.com](http://www.northropgrumman.litef.com) (2013).
- [4] Sensoror, “STIM300 IMU”, [www.sensoror.com](http://www.sensoror.com), (2014).
- [5] Analog Devices, “ADIS16445 Compact, Precision Six Degrees of Freedom Inertial Sensor”, [www.analog.com](http://www.analog.com) (2014).
- [6] ST Micro, “LSM330DLC iNEMO Inertial Module”, [www.st.com](http://www.st.com) (2012).
- [7] Invensense, “MPU-6500 Motion Tracking Device”, [www.invensense.com](http://www.invensense.com) (2014).
- [8] Fairchild, “FIS1100 MEMS Inertial Measurement Unit”, [www.fairchildsemi.com](http://www.fairchildsemi.com) (2015).
- [9] A. Efimovskaya, D. Senkal, Sina Askari, and A. M. Shkel, “Origami-Like Folded MEMS for Realization of TIMU: Fabrication Technology and Initial Demonstration”, *IEEE ISISS 2015*, Hapuna Beach, Hawaii, USA, March 23-26, (2015).
- [10] A. Efimovskaya, D. Senkal, A. M. Shkel, “Miniature origami-like folded MEMS TIMU”, *Proc. 18th Int. Solid-State Sensors, Actuators and Microsystems Conf. (Transducers’15)*, Alaska, USA, June 21-25, (2015).
- [11] R. N. Candler, M. A. Hopcroft, B. Kim, W-T. Park, R. Melamud, M. Agarwal, G. Yama, A. Partridge, M. Lutz, T. W. Kenny, “Long-Term and Accelerated Life Testing of a Novel Single-Wafer Vacuum Encapsulation for MEMS Resonators”, *JMEMS*, 15, (6), pp. 1446-1456, (2006).
- [12] D. Senkal, S. Askari, M.J. Ahamed, E. Ng, V. Hong, Y. Yang, C.H. Ahn, T. W. Kenny, A. M. Shkel, “100k Q-Factor Toroidal Ring Gyroscope Implemented in Wafer-level Epitaxial Silicon Encapsulation Process”, *IEEE MEMS 2014*, San Francisco, CA, USA, January 26-30, (2014).

## CONTACT

\* A. Efimovskaya, tel: +1-949-824-6314; [aefimovs@uci.edu](mailto:aefimovs@uci.edu)